Understanding the mechanical response of double-stranded DNA and RNA under constant stretching forces using all-atom molecular dynamics

Alberto Marin-Gonzalez[1†], J. G. Vilhena[1,2†], Ruben Perez[2,3*] and Fernando Moreno-Herrero[1*]

[1]Department of Macromolecular Structures, Centro Nacional de Biotecnología, Consejo Superior de Investigaciones Científicas, 28049 Cantoblanco, Madrid, Spain

[2]Departamento de Física Teórica de la Materia Condensada, Universidad Autónoma de Madrid, E-28049 Madrid, Spain

[3]IFIMAC - Condensed Matter Physics Center, Universidad Autónoma de Madrid, E-28049 Madrid, Spain

Supporting Information

Table of contents

[†]These two authors contributed equally to this work

[*]Correspondence should be addressed to ruben.perez@uam.es and fernando.moreno@cnb.csic.es

Supplementary Methods

1.- Obtaining the parameters of the elastic rod model

In the regime where bending fluctuations are negligible, the elastic energy of a NA can be written as (1-4)

$$E(x,\theta,F) = \frac{1}{2}\frac{C}{L}\theta^2 + g\theta\frac{x}{L} + \frac{1}{2}\frac{S}{L}x^2 - xF \quad \text{(S1)}$$

where L is the equilibrium extension at zero force, x is the elongation or deviation from L and θ is the change in helical twist from its unperturbed equilibrium value. The three parameters *S*, *C* and g are the stretch modulus, the twist modulus, and the twist-stretch coupling, respectively.

If F and θ are fixed (F_0,θ_0), the value of the extension (x^*) that minimizes the energy is given by(1, 2)

$$\left(\frac{\partial E}{\partial x}\right)_{F=F_0,\theta=\theta_0} = 0 \Rightarrow g\frac{\theta_0}{L} + \frac{S}{L}x^* - F_0 = 0 \Rightarrow x^* = \frac{L}{S}\left(F_0 - \frac{g\theta_0}{L}\right) \quad \text{(S2)}$$

By the same token, at fixed F and x

$$\left(\frac{\partial E}{\partial \theta}\right)_{F=F_0,x=x_0} = 0 \Rightarrow gx_0 + C\theta^* = 0 \Rightarrow \theta^* = -\frac{g}{C}x_0 \quad \text{(S3)}$$

Moreover, at a given value of the force there is a global minimum of the energy in (x,θ). We denote this minimum ($<x>$,$<\theta>$). We can take $\theta_0 = <\theta>$ in **Equation (S2)** and $x_0 = <x>$ in **Equation (S3)**, obtaining

$$<\theta> = -\frac{g}{C}<x> \quad \text{(S4)}$$

$$\frac{<x>}{L} = \frac{F}{S} - g\frac{<\theta>}{SL} \quad \text{(S5)}$$

By substituting the value of $<\theta>$ from **Equation (S4)** in **Equation (S5)**, one gets(1)

$$\frac{<x>}{L} = \frac{F}{S - g^2/C} \equiv \frac{F}{\tilde{S}} \quad \text{(S6)}$$

Substituting $<x>$ from **Equation (S6)** in **Equation (S4)** one obtains the following expression for the helical twist

$$\frac{<\theta>}{L} = -\frac{g}{C\tilde{S}}F \quad \text{(S7)}$$

Finally, a third relation can be obtained if the twisting angle imposed in **Equation (S2)** is changed while keeping the force constant. The equilibrium extension then varies as(2-4)

$$\left(\frac{\partial x^*}{\partial \theta_0}\right)_F = -\frac{g}{S} \quad \text{(S8)}$$

Hence, in order to compute the parameters of the elastic rod model one needs to measure three quantities: the dependence of the elongation (**Equation (S6)**) and the twisting angle (**Equation (S7)**) with the force and how thermal fluctuations of the twisting angle are coupled to fluctuations of the elongation (**Equation (S8)**). Notice that the equations are coupled, so the determination of the elastic parameters requires solving the system of equations.

We denote $A_1 \equiv 1/\tilde{S}$, $A_2 \equiv -g/\tilde{S}C$ and $A_3 \equiv -g/S$, obtaining

$$S = \frac{1}{A_1 - A_2 A_3} \tag{S9}$$

$$C = \frac{A_1 A_3 / A_2}{A_1 - A_2 A_3} \tag{S10}$$

$$g = -\frac{A_3}{A_1 - A_2 A_3} \tag{S11}$$

These equations allow us to compute all elastic parameters from the slopes of **Fig 2a** and **Fig. 2b** (A_1,A_2) and from the helical rise - helical twist slopes computed in **Fig. S3** (A_3).

For the sake of simplicity, $< x >$, x^* and x_0 are all denoted as x in the main text; the same holds for θ.

2.- Determining changes in extension from the springiness model

In a nucleic acid (NA), a chain of segments can be defined that joins the centers of all consecutive base pairs(4, 5) (**Fig. 3).** If bending is neglected, the extension of the molecule can be written as

$$h = h(l, \cos\beta) = l\cos\beta \tag{S12}$$

where l is the length of the chain and β is the angle defined by the chain with the helical axis (see next section for more details). Introducing an external force will induce a variation in these quantities

$$h(l(F), \cos\beta(F)) = l(F)\ \cos\beta(F) \tag{S13}$$

If the change in h induced by the force is small enough, we can write $h(F)$ as a Taylor expansion around $h(F=1) \equiv L$ and stay at the first order approximation. Denoting $l(F=1) \equiv l_0$, $\cos\beta(F=1) \equiv \cos\beta_0$, we get

$$\begin{aligned} h(F) - h(1) &\equiv x \\ &= \left(\frac{\partial h(l,\cos\beta)}{\partial l}\right)_{\substack{l=l_0 \\ \cos\beta=\cos\beta_0}} \Delta l + \left(\frac{\partial h(l,\cos\beta)}{\partial(\cos\beta)}\right)_{\substack{l=l_0 \\ \cos\beta=\cos\beta_0}} \Delta(\cos\beta) \\ &= \cos\beta_0 \Delta l + l_0 \Delta(\cos\beta) \end{aligned} \tag{S14}$$

In the equation above, the first term accounts for the change in extension coming from separating consecutive base pairs from each other. The second term measures the contribution from deforming the chain of segments, changing its end-to-end distance when the length of the segments is kept fixed. Consequently, we define these quantities as

$$x_{\Delta l} \equiv \cos\beta_0 \Delta l; \qquad x_{\Delta\beta} \equiv l_0 \Delta(\cos\beta) \tag{S15}$$

$$x = x_{\Delta l} + x_{\Delta\beta} \tag{S16}$$

As shown above (**Equation (S6)**), in the elastic rod model x varies linearly with the force as $x = (FL)/\tilde{S}$. Our results revealed that $x_{\Delta l}$ and $x_{\Delta\beta}$ also depend linearly on the force (**Fig. 3**). We express this as

$$\frac{x_{\Delta l}}{L} = \frac{F}{k_l}; \qquad \frac{x_{\Delta\beta}}{L} = \frac{F}{k_\beta} \tag{S17}$$

Then, from these two relations and **Equation (S1)** and **Equation (S6)**, we get

$$\frac{x}{FL} = \frac{1}{\tilde{S}} = \frac{1}{k_l} + \frac{1}{k_\beta} \Rightarrow \tilde{S} = \frac{k_l k_\beta}{k_l + k_\beta} \tag{S18}$$

This equation illustrates that we are just modelling the elastic response of NA as two springs in series of elastic constants k_l and k_β.

For the two molecules, x/L, $x_{\Delta l}/L$ and $x_{\Delta\beta}/L$ were plotted against the force and fitted to a linear function (**Fig. 3c**, main text). The inverse of the slopes are $\tilde{S}$, k_l and k_β, respectively. Finally, for consistency, we also computed $\tilde{S}$ from k_l and k_β using the **Equation (S18)**, in excellent agreement with the $\tilde{S}$ obtained directly from the x versus F slope. Results are shown in **Table S1**.

Force constant	dsDNA	dsRNA
k_l (pN)	5600(1500)	2170(140)
k_β(pN)	1330(50)	522(3)
$\tilde{S}$ (pN), measured	1120(50)	416(7)
$\tilde{S}$ (pN), from equation S18	1076(68)	421(15)

Table S1. Elastic constants of the springiness model determined for dsDNA and dsRNA.

3.- Quantifying the springiness from the MD simulations

At each simulation frame, $\cos\beta$ was defined as the sum of the helical rises of the nine central base pair steps divided by the sum of the distances between the centers of consecutive base pairs. In the 3DNA convention, the distance between two consecutive base pairs is the square root of the sum of the squares of the base pair step parameters shift, slide and rise(6, 7). All this can be expressed as

$$(\cos\beta)(t) \equiv \frac{\sum_i h_i(t)}{\sum_i l_i(t)} = \frac{\sum_i h_i(t)}{\sum_i \sqrt{Dx_i^2(t)+Dy_i^2(t)+Dz_i^2(t)}} \quad \text{(S19)}$$

where the sums are extended over the nine central base pair steps, $h_i(t)$ is the helical rise, $l_i(t)$ is the distance between the base pair centers and $\left(Dx_i(t), Dy_i(t), Dz_i(t)\right)$ are the parameters (shift, slide, rise) of the base pair step i at simulation time t. If we simply denote $h(t)$ the mean value of the helical rise of the nine central base pair steps at simulation time t, and similarly for $l(t)$, we get

$$h(t) = l(t) \cdot (\cos\beta)(t) \quad \text{(S20)}$$

The equilibrium value of the helical rise at each constant force simulation is

$$h_{eq}(F) = < h(t) > (F) = < l(t) \cdot (\cos\beta)(t) > (F) \quad \text{(S21)}$$

where the notation <> refers to an average over the simulation time. Notice that, in general, the right hand side of **Equation (S21)** is *not* equal to the product of the time averages, but has the form

$$< l(t) \cdot (\cos\beta)(t) > (F) = < l > (F) \cdot < \cos\beta > (F) + cov(l, \cos\beta)(F) \quad \text{(S22)}$$

being $cov(l, \cos\beta)(F)$ the covariance of the two variables at a given force. This covariance was found to be negligible at all forces under study. Only then, can we safely write

$$< h > (F) = < l > (F) \cdot < \cos\beta > (F) \quad \text{(S23)}$$

and make use of **Equation (S12)** with the equilibrium values of l and $\cos\beta$ measured from the simulations to compute h.

The validity of these approximations (negligible covariance and first order Taylor expansion) is shown in the **Tables S2** and **S3**. The highest deviation from the measured value (for dsRNA at 20 pN) is less than 0.04%. Therefore, we can use the values from **Tables S2** and **S3** to quantify the *springiness* of dsDNA and dsRNA.

F (pN)	h (Å), measured	l (Å)	$\cos\beta$	h (Å), using Equation (S14)
1	2.6850	3.7813	0.7103	
5	2.7100	3.7853	0.7162	2.7102
10	2.7461	3.8016	0.7226	2.7459
15	2.7743	3.8042	0.7295	2.7739
20	2.8064	3.8140	0.7360	2.8054

Table S2. Validation check of the springiness model approximations in **dsRNA.**

F (pN)	h (Å), measured	l (Å)	$\cos\beta$	h (Å), using Equation (S14)
1	3.0786	3.5621	0.8645	
5	3.0934	3.5652	0.8679	3.0934
10	3.1000	3.5603	0.8710	3.1002
15	3.1193	3.5697	0.8741	3.1194
20	3.1343	3.5785	0.8761	3.1341

Table S3. Validation chech of the springiness model approximations in **dsDNA**.

4.- Quantifying the effect of bending fluctuations in the MD simulations

On the length scale of the molecule used in this work bending fluctuations are negligible. This can be easily shown in the absence of external force. At first order, one can approximate the difference in free energy due to bending, ΔG_{bend}, as a parabolic function. If the polymer is assumed to be bent along the arc of a circle (8)

$$\Delta G_{bend} = \frac{2P}{L}\left(\frac{\theta}{2}\right)^2 K_B T \quad \text{(S24)}$$

where P is the bending persistence length, L is the contour length of the polymer, θ is the bending angle. From the Virial Theorem and the previous equation it follows that the expected angle of bending (8) is

$$< (\theta/2)^2 > = \frac{L}{2P} \quad \text{(S25)}$$

We are analyzing 9 base pair steps with a mean helical rise of around 0.31nm, which yields $L = 9 * 0.31nm \cong 2.8nm$. Taking P as 50 nm (8) one obtains $< (\theta/2)^2 >= 0.028$ rad.

Assuming inextensibility, the effect of bending can be quantified as the ratio of the expected end-to-end distance (z) divided by the contour length of the polymer (L). The end-to-end distance and the contour length can be expressed in terms of the radius of curvature R_c and θ

$$z = 2R_c \sin(\theta/2) \;\; L = R_c\theta \quad \text{(S26)}$$

$$L = R_c\theta \quad \text{(S27)}$$

Substituting L in the first equation and writing the $\sin(\theta/2)$ as a Taylor expansion, one gets

$$\frac{z}{L} = \frac{\sin(\theta/2)}{\theta/2} \cong \frac{\theta/2 - \frac{(\theta/2)^3}{3!}}{\theta/2} = 1 - \frac{(\theta/2)^2}{6} \quad \text{(S28)}$$

Therefore, the effect of bending can be quantified as

$$\frac{<z>}{L} = 1 - \frac{<(\theta/2)^2>}{6} \quad \text{(S29)}$$

This yields for our molecule length a ratio of 0.995, and this justifies neglecting bending at the considered length scale. Furthermore, when applying force, bending fluctuations are suppressed and therefore they shall contribute even less to the total error on the elongation of the molecule.

5.- Comparing Curves+ and 3DNA as software analysis of MD simulations of NA

Two different software programs have been widely used to analyze the structural parameters of nucleic acids: Curves+ and 3DNA. Differences between these software programs applied to structures close to canonical B- and A-DNA have been reported to be very small, not exceeding ~0.1 Å for translational and ~2° for angular parameters (9). Since in this work we worked also with structures close to B and A conformations, we expected, and have confirmed, that this small discrepancy holds. This was also confirmed in (10), where Liebl et al. computed the helical-twist *vs* helical-rise slope using both software packages, finding very similar values for both dsDNA and dsRNA.

However, we chose 3DNA for most of our analysis for technical reasons. In the 3DNA convention the distance between the centers of consecutive base pairs is the square root of the sum of the squares of the translational base pair step parameters (**Equation (S19)**). This relation is needed for a mathematically consistent derivation of the *springiness* model in terms of the structural parameters.

dsDNA

Parameter	Curves+	3DNA	Literature
h-rise ($\AA$)	3.20	3.07	3.4 (11)
h-twist (deg)	31.96	32.87	36 (11)
$S\ (pN)$	1090	1280	1450-1750*
$\tilde{S}\ (pN)$	985	1120	649-1401*
$C\ (pN\ nm^2)$	256	303	386-448*
g/k_BT (unitless)	-40	-54	-(17-39)*

Table S4. Helical Rise, helical twist and elastic parameters measured for **dsDNA** using Curves+ and 3DNA software. * See references in **Table I**, main text.

dsRNA

Parameter	Curves+	3DNA	Literature
h-rise ($\AA$)	2.80	2.68	2.55 (11)
h-twist (deg)	31.25	32.08	33 (11)
$S\ (pN)$	429	480	
$\tilde{S}\ (pN)$	382	416	350,500*
$C\ (pN\ nm^2)$	298	310	409*

g/k_BT (unitless)	29	34	11.5*

Table S5. Helical Rise, helical twist and elastic parameters measured for **dsRNA** using Curves+ and 3DNA software. * See references in **Table I**, main text.

6.- Comparing our value of the dsRNA twist-stretch coupling with the one reported in Ref. (10)

We obtained higher values of the dsRNA's helical twist – helical rise slope (twist-stretch coupling) than those reported in Liebl et al. With the aim to better understand the reason of this discrepancy, we have carefully explored several aspects of our simulations that may potentially affect the magnitude of the twist-stretch coupling. We have concluded that this discrepancy can be traced down to a combination of different aspects regarding the processing software, the different force regime, and the inclusion of data in the non-linear regime to obtain average values.

The processing software

Liebl et al. compute the helical twist - helical rise slope from a linear regression of the these parameters obtained using the software **Curves+**. In our work, we have used the software **3DNA**. We have systematically reprocessed our data using Curves+ in order to compare both results. In general, both analysis software give similar nucleic acids values with some small differences that do not clearly benefit one of the two choices. **Table S4** includes all DNA/RNA parameters obtained with Curves+ and 3DNA. Regarding the value of g/S, Curves+ provides a value of the slope (helical twist - helical rise) slightly closer to the one reported in Liebl et al. (**Table S5**).

The external force

Liebl at al. performed simulations with zero stretching force. We have repeated the simulation for dsRNA with no force acting on the molecule, i.e., totally unrestrained molecules. When combined with the use of Curves+ as processing software the value of the slope got even closer to the value reported in Liebl et al. (**Table S6**)

Liebl et al.	**Software: 3DNA** **Force: 1pN**	**Software: Curves+** **Force: 1pN**	**Software: Curves+** **Force: F = 0 pN**
-0.037	-0.051	-0.048	-0.043

Table S6. Summary of g/S (Å/deg) values for dsRNA obtained with Curves+ and 3DNA at 1 pN and 0 pN force.

Non linear regime

The remaining difference may be attributed to the non-linearities reported in **Figure 5**, main text. As shown in that figure, the dependence of the helical twist with the helical rise for dsRNA is much more non-linear than for dsDNA. This results in that the high energy states

associated with these non-linearities, that are very hard to sample, have a high impact on the value of the slope. Consequently, a slight change in the sampling of this region induces a considerable change in the slope, making the value of the twist-stretch coupling very sensitive to the simulation conditions and processing analysis.

The Force Field

Finally, we have discarded the force field as potential source of discrepancy as we believe both studies use the same force-field, which for RNA consists on: parmbsc0 (ff99 + bsc0 refinement (12) + χOL3 modification (13). We have updated some details of the force field in the methods section of the main text, and added reference to the new section in Supplementary Information.

7.- Salt dependence of elastic parameters $\tilde{S}$ and g/S for dsDNA and dsRNA

In order to check how our measurement of $\tilde{S}$ and g are affected by different salt concentrations, we have performed a set of control simulations at 150 mM NaCl. Three simulations of about 1 μs were run for dsDNA and dsRNA at this salt condition and forces of 5, 15 and 20 pN.

We computed the helical rise for zero and 150 mM NaCl in both molecules (**Fig. S4**). For dsDNA, we found similar values for helical rise for both salt conditions at low forces and an increase in the stretch modulus as the force increases, consistent with the trend reported in (14) (15). The stretch modulus was inferred from the inverse of the slope multiplied by a reference extension taken as the extension given by the fit at 1 pN force, as we did in the main text. For dsRNA, however, helical rise values were systematically lower than those calculated at zero salt and closer to the extension per base pair of the crystallized A-type helix (~2.6Å). This may be explained by the fact that the A-form structure (dsRNA) accumulates more counterions than the B-form (dsDNA) as suggested in (16). However, the calculation of the stretch modulus of dsRNA in these conditions gave a value consistent with that reported in (15). Calculated stretch modulus are reported in **Table S7.**

Still, in order to investigate if our zero salt conditions may explain the discrepancy of the twist stretch coupling between the experimental value reported and our simulations we have also computed the ratio $-g/S$ at different forces for both molecules at 150 mM NaCl (**Fig. S4**). We obtained very similar values at all forces with respect to neutralizing salt conditions with deviations below 10%.

These data indicate that salt concentration is not the primary reason for the discrepancies observed when comparing $-g/S$ with experimental data and validates our approach with neutralizing salt conditions to investigate mechanical properties of nucleic acids.

[NaCl]	dsDNA	dsRNA
0mM	1120 (50)	416(7)
150mM	1540 (160)	420 (20)

Table S7. Twist-unrestrained stretch modulus, $\tilde{S}$, at 0 mM and 150 mM of NaCl for dsDNA/dsRNA. The twist-unrestrained stretch moduli were computed from the inverse of the slopes of **Fig. S4**. The higher value of $\tilde{S}$ at 150 mM with respect to the neutralizing salt simulation is consistent with the trend of increasing the stretch modulus with the NaCl concentration reported for dsDNA and dsRNA in (15).

8.- Measurement of inter-strand separation from MD simulations

The inter-strand separation was measured in three different ways: i), as twice the radial components of the gyration tensor of the P-atoms, ii), as twice the mass-weighted radial components of the gyration tensor of all the atoms of the backbone and, iii), using the formula for the radius provided in (17). The following provide details on the procedure to perform these measurements.

1. **The radial components of the gyration tensor of the P-atoms.** The crystallized B-DNA (or A-RNA) initial configuration was centered by imposing its helical axis to run along the *z*-axis of the Amber coordinates. Using the command *rms* of the *cpptraj* software, each constant force trajectory was aligned with respect to the centered B-DNA (A-RNA) structure. Then, using the command *radgyr* of *cpptraj* the gyration tensor was computed for the P-atoms of the 10 central base pairs. Since the molecules are double helices with a helical pitch close to 10 base pairs, values of the *xx* and *yy* components of the gyration tensor were very similar, confirming the isotropy in the *x*-*y* plane. The average distance of the P-atoms to the helical axis was computed as the square root of the sum of the *xx* and *yy* components of the gyration tensor for a given frame. This was averaged for all frames over the entire simulation time (**Fig. S6a**).

2. **The radial components of the mass-weighted gyration tensor of all backbone atoms.** This procedure is similar to the previous one with the only difference being that the gyration tensor is computed for all the atoms of the backbone with weights proportional to their masses instead of only using the P-atoms (**Fig. S6a**).

3. **Theoretical formula for the helical radius.** In Kosikov et al. (17) a theoretical formula is provided for helical radius

$$R = \langle \sqrt{\left(d_{pp}^2 - h^2\right)/2\left(1 - cos(\theta + \theta_0)\right)} \rangle \qquad \text{(S30)}$$

where d_{pp}, h, and $\Omega_{\mathrm{h}} = \theta + \theta_0$ are, respectively, the distance between consecutive phosphates of the same strand, the helical rise and the helical twist. In the expression above we are considering the average of these parameters for the nine central base

pair steps at a given simulation frame. The angular brackets denote an average over the simulation time (**Fig. S6b**).

Values of the inter-strand distance using only the P-atoms (method 1 and 3) yielded very similar results, confirming the soundness of both methodologies (**Fig. S6c, upper panels**). Interestingly, the distance of the P-atoms to the helical axis was found to be larger for dsDNA than for dsRNA, in apparent contradiction with the well known picture of dsDNA as a narrower helix than dsRNA. However, a top view of the crystallized B-DNA and A-RNA structures (**Fig. S6a**) reveals that although the backbone atoms are generally further from the helical axis for dsRNA than for dsDNA, the P-atoms are indeed closer to this axis in the former. Indeed, if all the atoms of the backbone are considered, one obtains the expected broader form of dsRNA (**Fig. S6c, upper panels**).

Despite this difference found in the absolute values of the inter-strand separation of the molecules depending on whether one considers all the backbone atoms (method 2) or only the P-atoms (method 1 and 3), the relative change in the inter-strand distance was found to be very similar regardless of the methodology used (**Fig. S6c, lower panels**). This indicates that, in this range of forces, the dynamics of the strands can be well described by their heaviest atoms, i.e. the phosphorus, and supports the use of any of the described methodologies to calculate the inter-strand distance.

9.- Simulation Details

NA duplexes were built using the software NAB (7). NA sequences were d(5'-GCGCAATGGAGTACGC/5'-GCGTACTCCATTGCGC) for dsDNA and r(5'-GCGCAAUGGAGUACGC/5'-GCGUACUCCAUUGCGC) for dsRNA, following the work of Liebl et al. (Ref. (10)). Molecules were neutralized with sodium counterions and no additional salt was added. The systems were then placed in a box of dimensions 80Å x 80Å x 80Å filled with explicit water molecules. Both systems were energy-minimized in 5000 steps with restraints on the NA followed by 5000 steps of unrestrained minimization. Then, the systems were heated up to 300 K and equilibrated for 20 ns in the isobaric-isothermal (NPT) ensemble (P = 1 atm, T = 298 K). After NPT equilibration, and starting from the last configuration of the equilibration, five simulations were run for dsDNA and dsRNA at constant forces of 1, 5, 10, 15 and 20 pN in the NVT ensemble. The first 200 ns were taken as constant-force equilibration and all the measurements were performed on the last 800 ns. Following Ref. (10), only the ten central base pairs were considered for the data analysis.

We used the AMBER14 software suite (7) with NVIDIA GPU acceleration (18-20). The parmbsc0 (12) and the χOL3 modification (13) of the Cornell ff99 force field (21) was used to describe dsDNA and dsRNA. Water was described using the TIP3P model (22), while Joung/Cheatham parameters were used to describe the sodium counter-ions (23, 24). Periodic boundary conditions and Particle Mesh Ewald (with standard defaults and a real-space cutoff of 9Å) were used to account for long-range electrostatic interactions. Van der Waals contacts

were truncated at the real space cutoff. SHAKE algorithm was used to constrain bonds containing hydrogen, thus allowing us to use an integration step of 2 fs. Coordinates were saved every 1000 steps.

10.- Data processing

Data processing was carried out using the software Ambertools. Helical rise, helical twist, and base pair parameters were averaged over the ten central base pairs and over the last 800 ns of the simulation. Watson-Crick h-bonds were calculated for each frame of the simulation.

Simulation values and errors in **Fig. 2**, **Fig. 3c** , and **Fig. 4b** were calculated as follows. We split the simulations in five consecutive time windows of 160 ns. For each time window, we calculated the corresponding mean simulation value. Discrete data in the plots are the mean value and the standard error of the mean considering the five time windows. This procedure aims to mimic the typical experimental methodology where multiple independent measurements are usually taken.

11.- Constant force protocol

Latest versions of the Amber software package (7) allow the implementation of a restraint more sophisticated than the standard parabolic function. This more complicated form of the potential is described by six parameters: r_1, r_2, r_3, r_4, rk_2, and rk_3, where $r_1 < r_2 < r_3 < r_4$ and $rk_2, rk_3 > 0$. The $r_i´s$ split the space of the restraining coordinate R in five regions. The restraint energy E_{res} (**Fig. S14**) is given by the piecewise-defined function:

$$E_{res}(R) = \begin{cases} A_1 R + B_1 & \text{if } R \leq r_1 \\ rk_2(R - r_2)^2 & \text{if } r_1 < R \leq r_2 \\ 0 & \text{if } r_2 < R \leq r_3 \\ rk_3(R - r_3)^2 & \text{if } r_3 < R \leq r_4 \\ A_2 R + B_2 & \text{if } R > r_4 \end{cases} \quad \text{(S31)}$$

where A_1, B_1, A_2 and B_2 can be easily computed by imposing continuity in $E_{res}(R)$ and its derivative. Here we only need A_1, which can be obtained from the condition

$$\left(\frac{dE_{res}}{dR}\right)_{R=r_1^+} = \left(\frac{dE_{res}}{dR}\right)_{R=r_1^-} \Rightarrow A_1 = 2rk_2(r_1 - r_2) = -2rk_2(r_2 - r_1) < 0 \quad \text{(S32)}$$

Hence, in the region $R \leq r_1$ the potential is linear with a negative slope. If the restraining coordinate is a distance, the potential is translated into a force acting on the atoms chosen for the restraint. In the region $R \leq r_1$ this force is

$$\vec{F} = -\vec{\nabla}\mathrm{E_{res}(R)} = -\frac{\mathrm{dE_{res}}}{\mathrm{dR}}\vec{\mathrm{u}}_\mathrm{R} = -\mathrm{A_1}\vec{\mathrm{u}}_\mathrm{R} = 2rk_2(r_2 - r_1)\,\vec{\mathrm{u}}_\mathrm{R} \quad \text{(S33)}$$

where $\vec{\mathrm{u}}_\mathrm{R}$ is a unit vector along the direction of the line joining the restrained atoms. This equation illustrates that the force *i)* is constant in modulus, *ii)* always has the direction of the line joining the restrained atoms ($\vec{\mathrm{u}}_\mathrm{R}$) and *iii)*, is positive, meaning that it points outwards the

two restrained atoms. Altogether, this results in a constant stretching force.

In our constant force simulations the restrains were applied to the center of mass of the C1' atoms of the second and the fifteenth base pairs. This choice has been used before to restrain the twisting angle of the molecule (10, 25). In our case, the value of r_1 was chosen to be large enough for the restraining coordinate to remain in the first region $R < r_1$ at every simulation frame. The values of r_1, and r_2 were the same for all constant force simulations and by only modifying the value of rk_2 we tuned the value of the stretching force.

12.- Supplementary References

1. Marko JF (1997) Stretching must twist DNA. *Europhys. Lett.* **38,** 183.
2. Gore J, et al. (2006) DNA overwinds when stretched. *Nature* **442,** 836-9.
3. Lionnet T, Joubaud S, Lavery R, Bensimon D, Croquette V (2006) Wringing out DNA. *Phys Rev Lett* **96,** 178102.
4. Lipfert J, et al. (2014) Double-stranded RNA under force and torque: similarities to and striking differences from double-stranded DNA. *Proc Natl Acad Sci U S A* **111,** 15408-13.
5. Chou FC, Lipfert J, Das R (2014) Blind predictions of DNA and RNA tweezers experiments with force and torque. *PLoS Comput Biol* **10,** e1003756.
6. Lu XJ, Olson WK (2003) 3DNA: a software package for the analysis, rebuilding and visualization of three-dimensional nucleic acid structures. *Nucleic Acids Res* **31,** 5108-21.
7. Case DA, et al. (2014) *Amber14, University of California, San Francisco, CA.*
8. Bloomfield VA, Crothers DM, Tinoco I (2000) *Nucleic Acids: Structures, Properties and functions* (University Science Books, Sausalito, California).
9. Lavery R, Moakher M, Maddocks JH, Petkeviciute D, Zakrzewska K (2009) Conformational analysis of nucleic acids revisited: Curves+. *Nucleic Acids Res* **37,** 5917-29.
10. Liebl K, Drsata T, Lankas F, Lipfert J, Zacharias M (2015) Explaining the striking difference in twist-stretch coupling between DNA and RNA: A comparative molecular dynamics analysis. *Nucleic Acids Res* **43,** 10143-56.
11. Sinden RR (1994) *DNA structure and function* (Academic Press, London).
12. Perez A, et al. (2007) Refinement of the AMBER force field for nucleic acids: improving the description of alpha/gamma conformers. *Biophys J* **92,** 3817-29.
13. Zgarbova M, et al. (2011) Refinement of the Cornell et al. Nucleic Acids Force Field Based on Reference Quantum Chemical Calculations of Glycosidic Torsion Profiles. *J Chem Theory Comput* **7,** 2886-2902.
14. Baumann CG, Smith SB, Bloomfield VA, Bustamante C (1997) Ionic effects on the elasticity of single DNA molecules. *Proc Natl Acad Sci U S A* **94,** 6185-90.
15. Herrero-Galan E, et al. (2013) Mechanical identities of RNA and DNA double helices unveiled at the single-molecule level. *J Am Chem Soc* **135,** 122-31.
16. Chen AA, Marucho M, Baker NA, Pappu RV (2009) Simulations of RNA interactions with monovalent ions. *Methods Enzymol* **469,** 411-32.
17. Kosikov KM, Gorin AA, Zhurkin VB, Olson WK (1999) DNA stretching and compression: large-scale simulations of double helical structures. *J Mol Biol* **289,** 1301-26.

18. Salomon-Ferrer R, Gotz AW, Poole D, Le Grand S, Walker RC (2013) Routine Microsecond Molecular Dynamics Simulations with AMBER on GPUs. 2. Explicit Solvent Particle Mesh Ewald. *J Chem Theory Comput* **9,** 3878-88.

19. Gotz AW, et al. (2012) Routine Microsecond Molecular Dynamics Simulations with AMBER on GPUs. 1. Generalized Born. *J Chem Theory Comput* **8,** 1542-1555.

20. Le Grand S, Gotz AW, Walker RC (2013) SPFP: Speed without compromise—A mixed precision model for GPU accelerated molecular dynamics simulations. *Computer Physics Communications* **184,** 374-380.

21. Cornell WD, et al. (1995) A Second Generation Force Field for the Simulation of Proteins, Nucleic Acids, and Organic Molecules. *J. Am. Chem. Soc.* **117,** 5179-5797.

22. Jorgensen WL, Chandrasekhar J, Madura JD, Impey RW, Klein M (1983) Comparison of simple potential functions for simulating liquid water. *J. of Chemical Physics* **79,** 926.

23. Joung IS, Cheatham TE, 3rd (2009) Molecular dynamics simulations of the dynamic and energetic properties of alkali and halide ions using water-model-specific ion parameters. *J Phys Chem B* **113,** 13279-90.

24. Li P, Roberts BP, Chakravorty DK, Merz KM, Jr. (2013) Rational Design of Particle Mesh Ewald Compatible Lennard-Jones Parameters for +2 Metal Cations in Explicit Solvent. *J Chem Theory Comput* **9,** 2733-2748.

25. Kannan S, Kohlhoff K, Zacharias M (2006) B-DNA under stress: over- and untwisting of DNA during molecular dynamics simulations. *Biophys J* **91,** 2956-65.

26. Gross P, et al. (2011) Quantifying how DNA stretches, melts and changes twist under tension. *Nature Physics* **7,** 731.

13.- Supplementary Figures

Figure S1

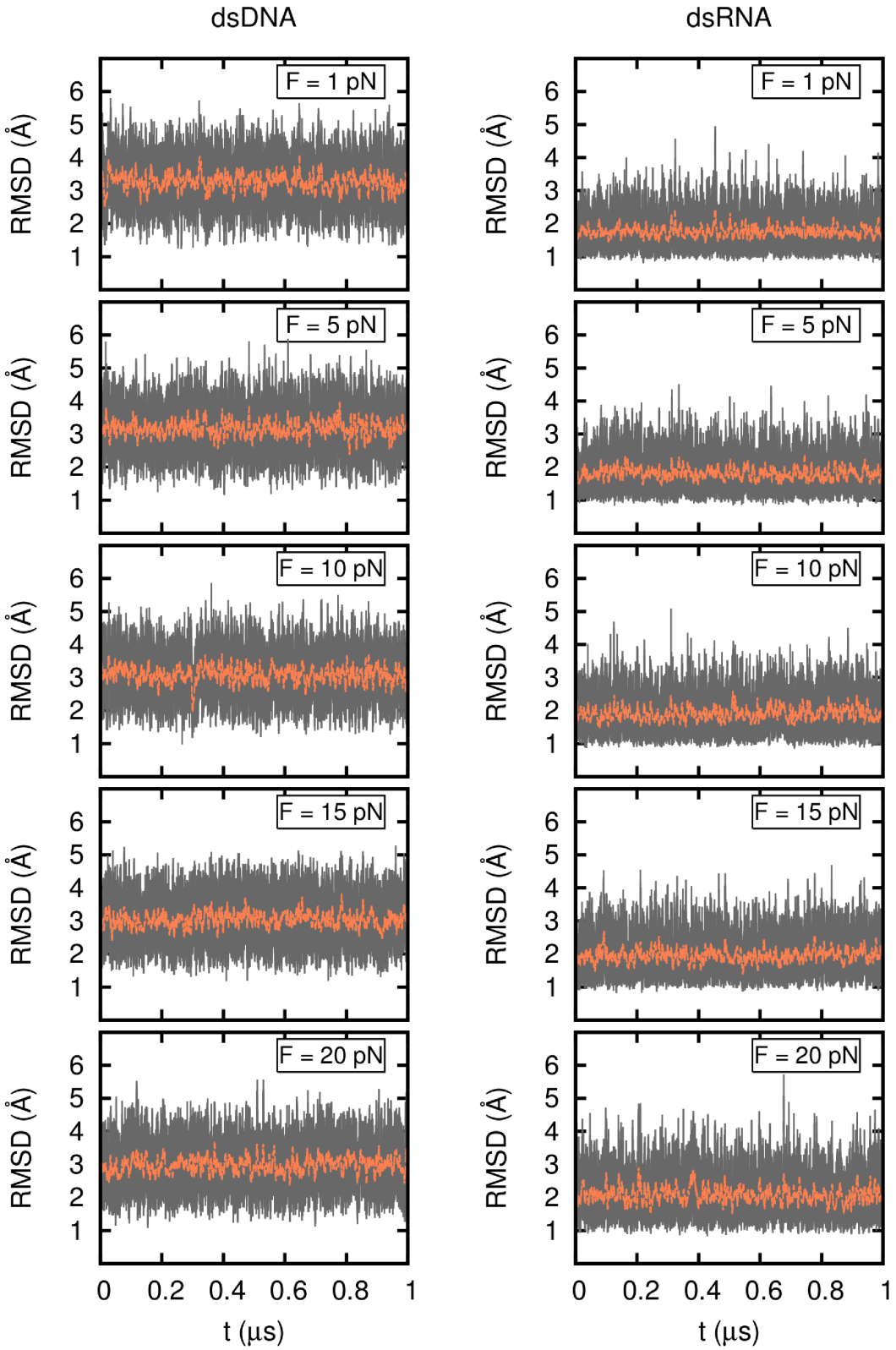

Figure S1: RMSD for dsDNA and dsRNA at different forces. The RMSDs were computed using the software AmberTools(7) for all heavy atoms with respect to the standard B-DNA and A-RNA starting configurations. Gray: RMSD at every simulation frame (1000 steps of 2 fs); red: data averaged over a running window of 2000 frames.

Figure S2

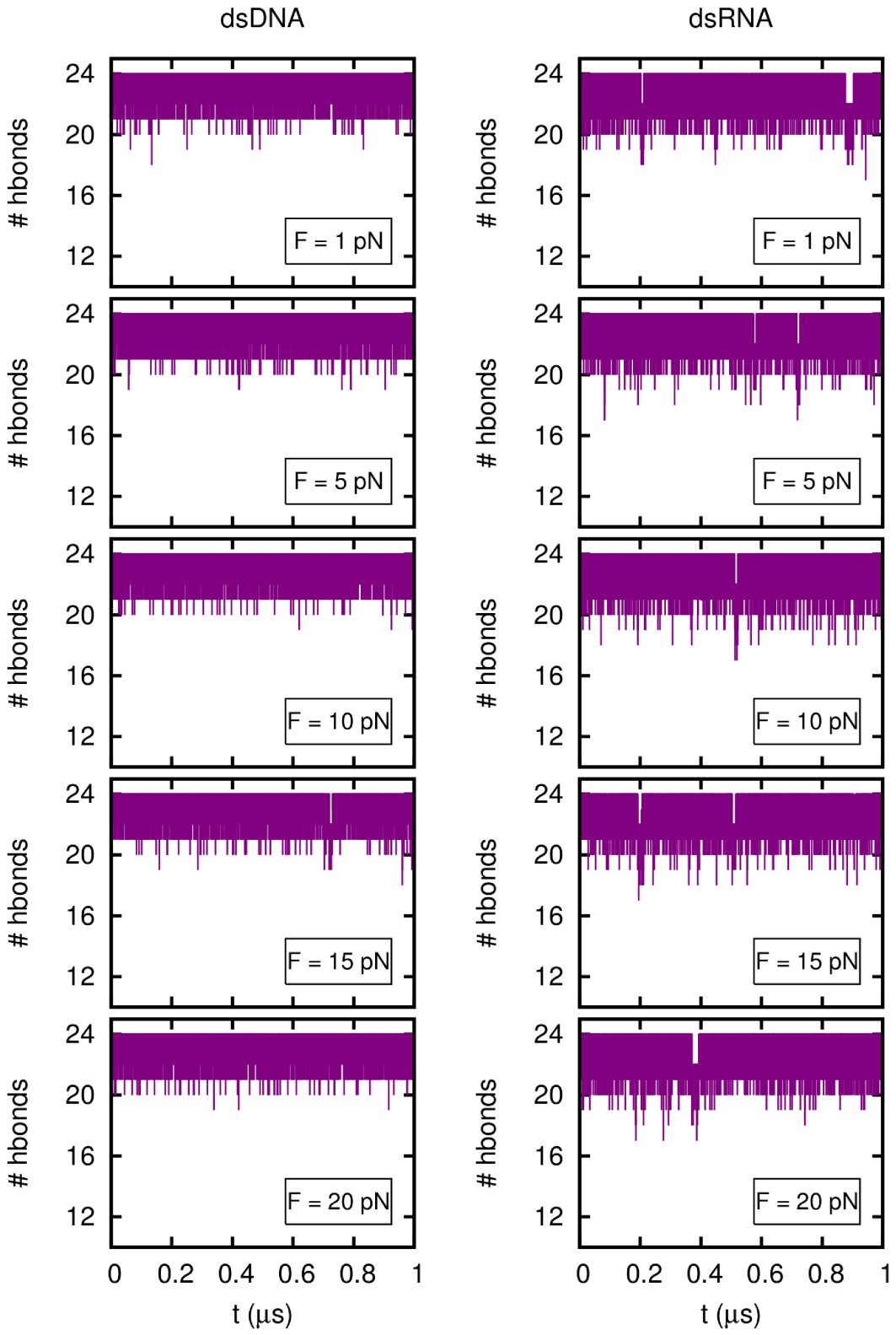

Figure S2: Number of Watson-Crick hydrogen bonds for dsDNA and dsRNA at different forces. The cut-off distance for the formation of an H-bond is 3.5 Å. The maximum, 24, corresponds to a configuration where all Watson-Crick H-bonds are formed.

Figure S3

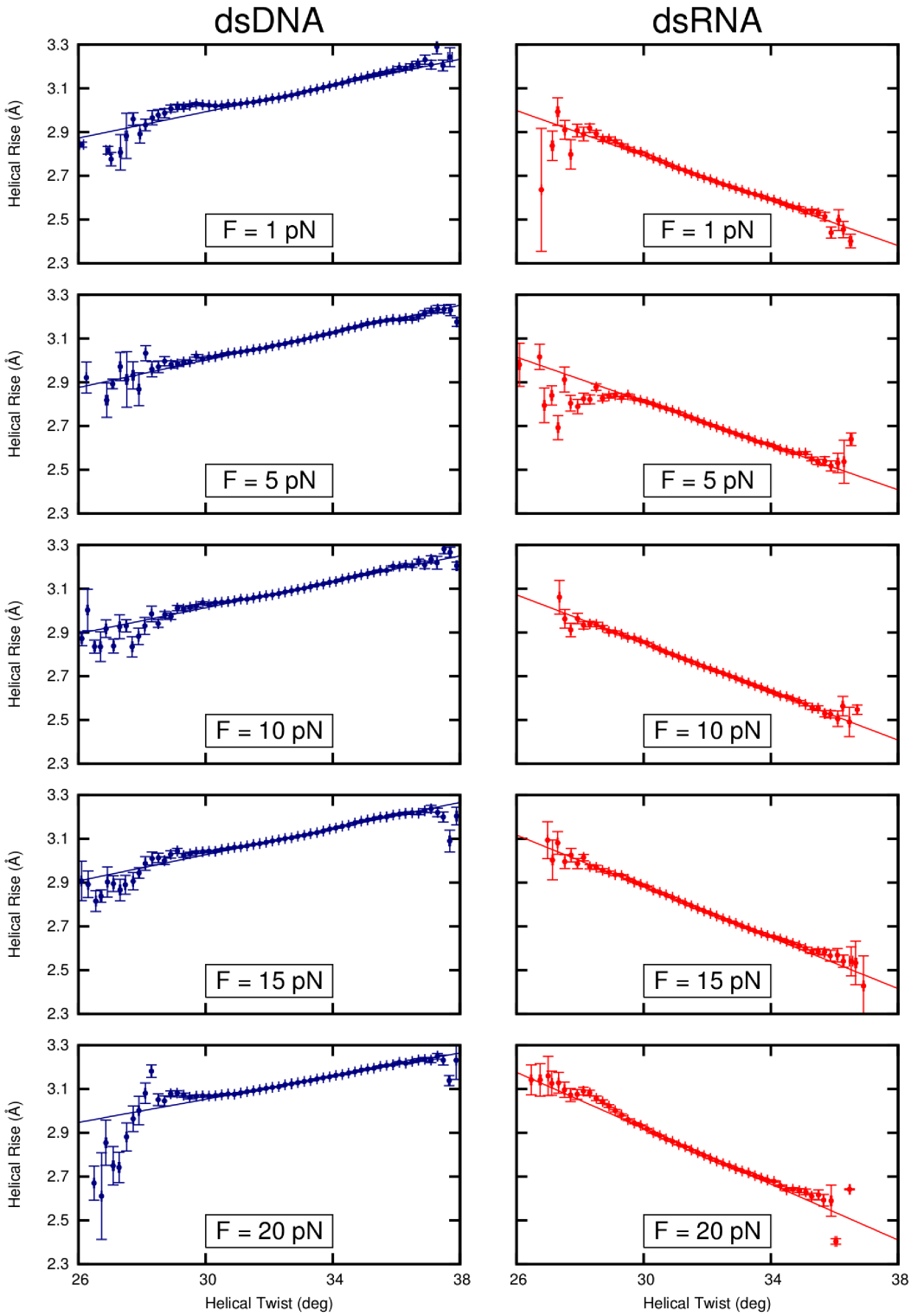

Figure S3: Helical rise - helical twist slopes at different forces for dsDNA/dsRNA. The helical twist and helical rise were computed using Ambertools (7). The mean helical twist and helical rise of the nine central base pair steps were computed for each simulation frame giving a total of 400000 points. The slopes were computed by fitting the raw data, i.e. the 400000 points. For representation purposes and following Ref. (10) the helical twist was discretized in bins of width of 0.2 degrees and the mean helical rise and helical twist was computed in each bin. Error bars are the standard error of the mean in each bin. Note that a fit to the discretized data would overweight the low populated events obtained at the extreme values of helical twist.

Figure S4

a

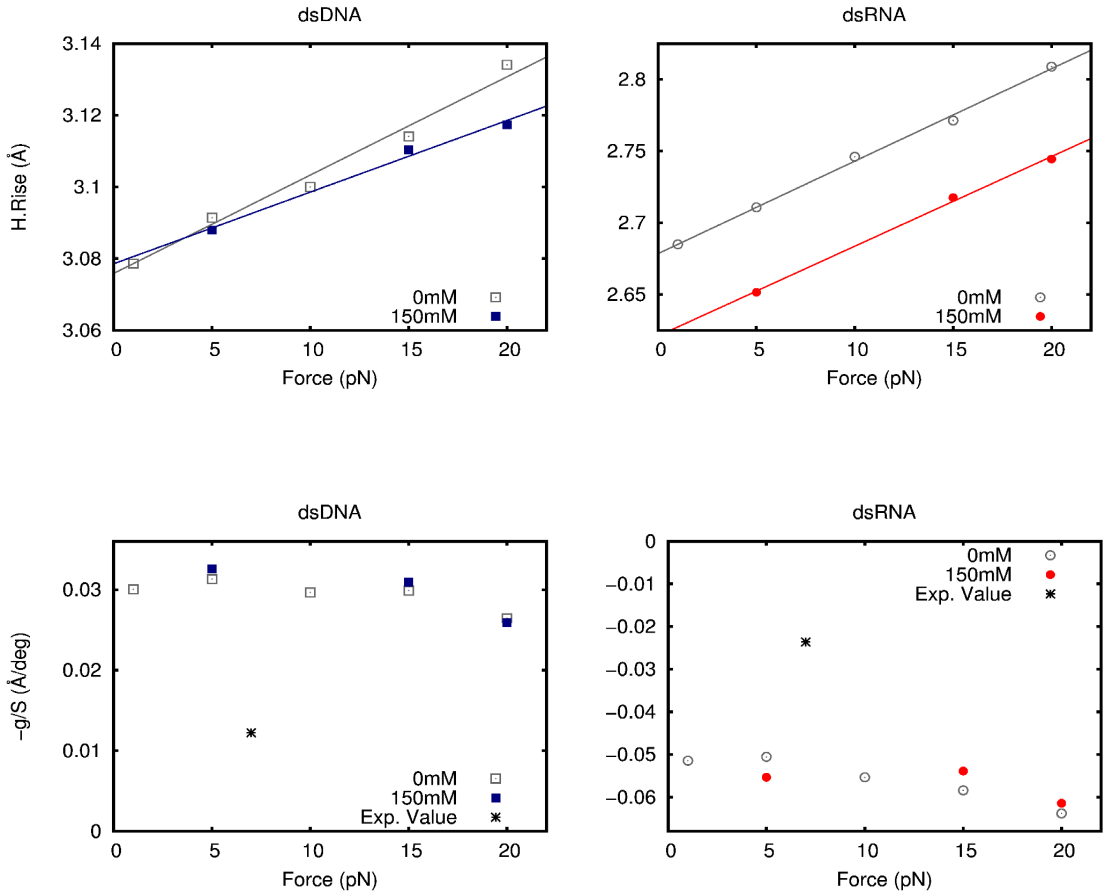

Figure S4: Control force-extension curves and helical twist-helical rise slopes for dsDNA and dsRNA at 0mM and 150mM of NaCl. **a**, the mean helical rise was computed at different forces for dsDNA/dsRNA in the same way as in **Figure 2a**, main text. Grey empty squares (circles) are the data at neutralizing salt (same data as in **Figure 2a**, main text) and filled blue (red) squares (circles) the data at 150mM for dsDNA (dsRNA). The stretch modulus was inferred from the inverse of the slope multiplied by a reference extension taken as the extension given by the fit at 1 pN force, resembling the procedure described in the main text. **b**, the ratio -g/S was computed for dsDNA/dsRNA in the same way as in **Figure 2c**, main text. Grey empty squares (circles) are the data at neutralizing salt (same data as in **Figure 2c**, main text) and filled blue (red) squares (circles) the data at 150mM for dsDNA (dsRNA). The black star represents the value of the slope measured at F = 7pN in (4).

Figure S5

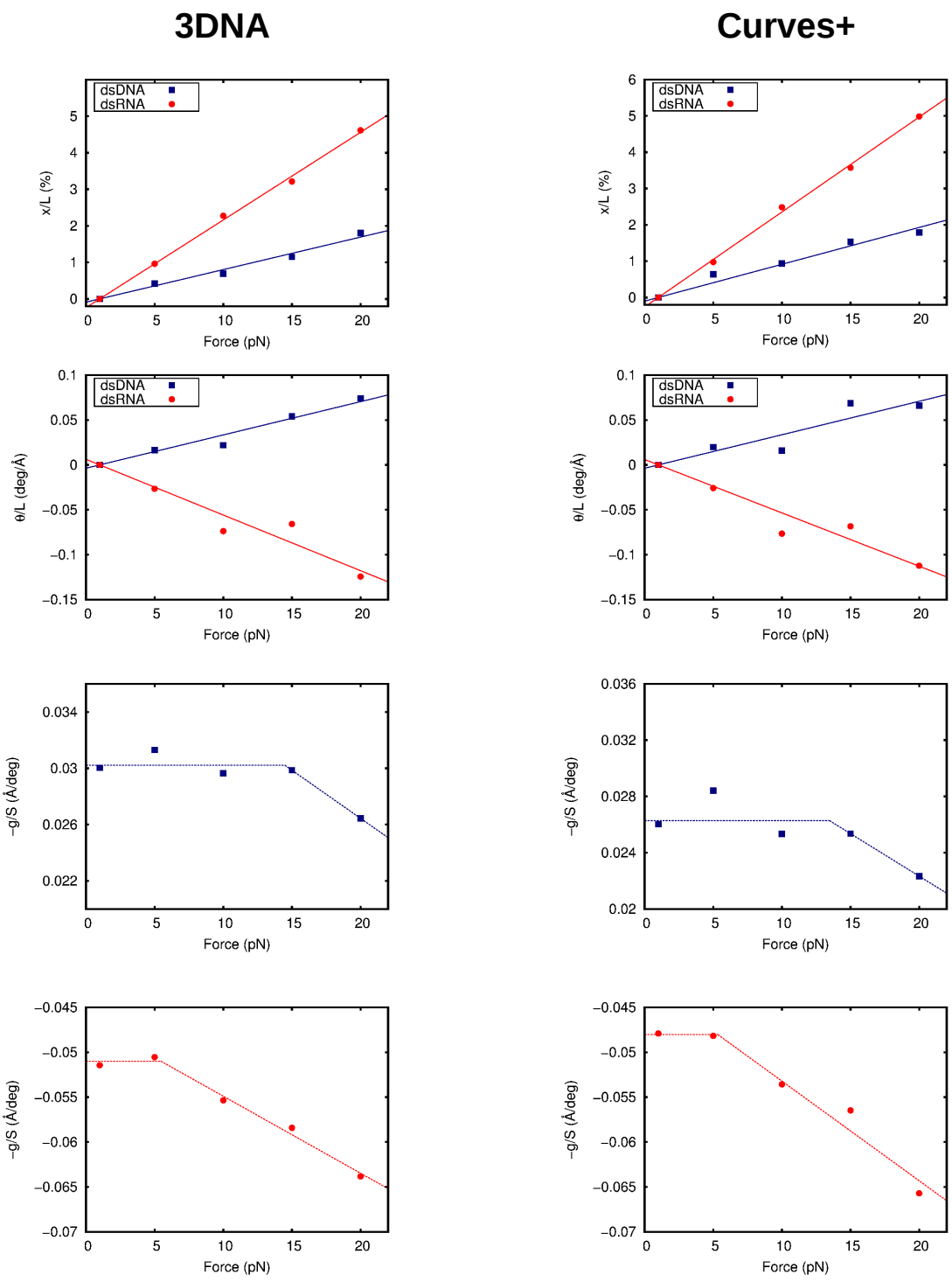

Figure S5: Comparison of dsDNA/dsRNA elastic parameters from MD data analysed with two different processing softwares: 3DNA and Curves+. In the left column we represent the results obtained using 3DNA, which were also shown in **Fig. 2** of the main text. In the right column we represent the same data processed using Curves+. Overall, very similar results are obtained which is also reflected in the similar values of the elastic parameters calculated from the fits to these plots (**Tables S4** and **S5**).

Figure S6

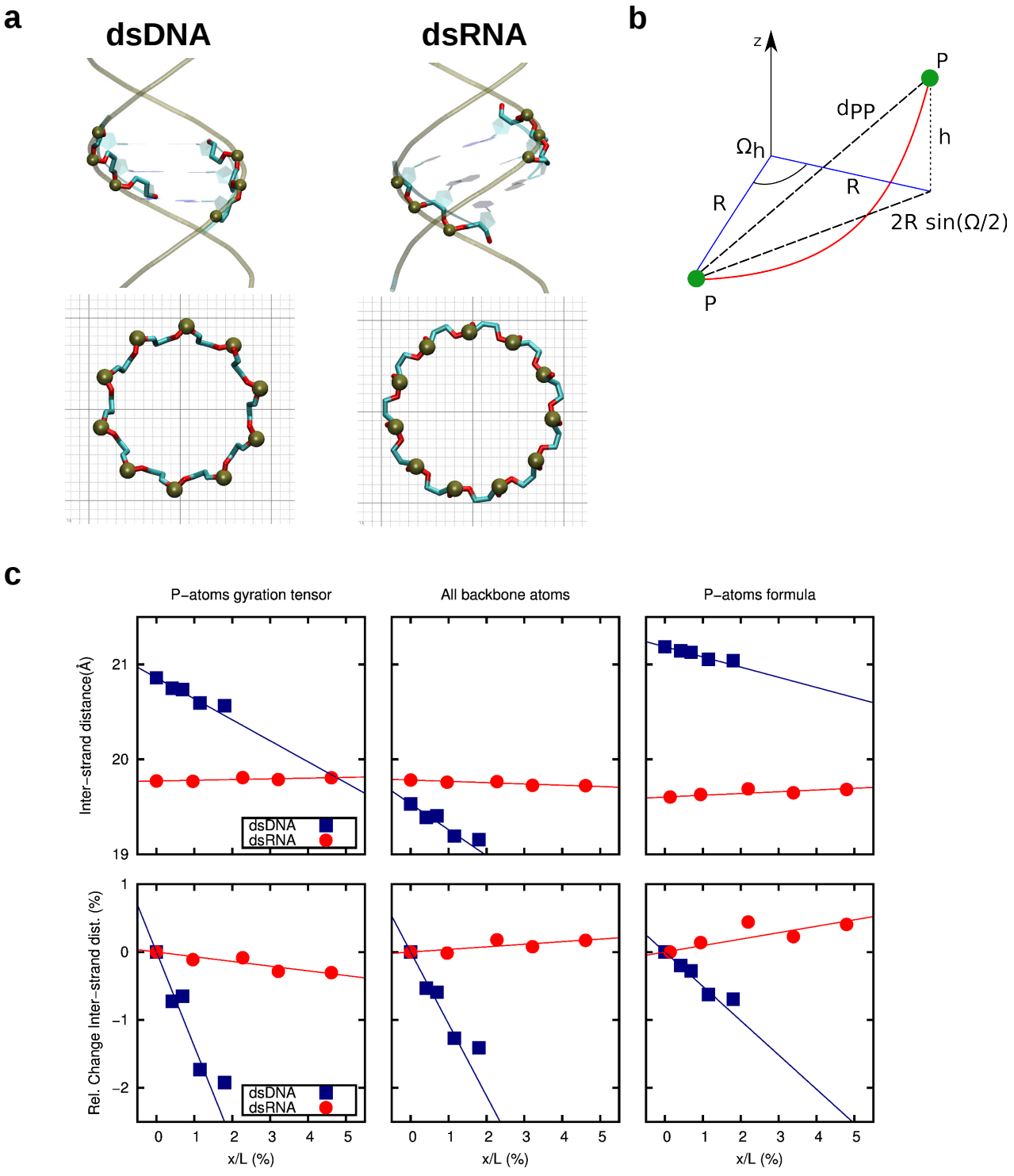

Figure S6: Inter-strand distance measurement. **a**, side and top views of dsDNA and dsRNA showing the position of P-atoms along the backbone. In the side view we included only three base-pairs. The smooth line represents the curve passing through the P-atoms (gold). The backbone atoms are represented by solid turquoise (C-atoms) and red (O-atoms) lines with the P-atoms highlighted as gold beads. **b**, Geometrical representation of the formula for the helical radius provided in (18). According to this formula the radius can be calculated as a function of the distance between consecutive phosphates, d_{PP}, the helical rise, h, and the helical twist $\Omega_h = \theta + \theta_0$. **c**, Change in inter-strand distance with the force-induced elongation for dsDNA and dsRNA using the three different measurements described in the Supporting Information. Top panel: the value of the inter-strand distance plotted versus the relative change in extension with respect to the F = 1pN value. Lower panel: relative change in inter-strand distance with respect to the F = 1 pN value plotted against the relative change in extension. A linear fit was performed for all data points in the case of dsRNA and excluding the point corresponding to F = 20pN in the case of dsDNA. For the relative change in inter-strand distance this fit was constrained to go through the origin.

Figure S7

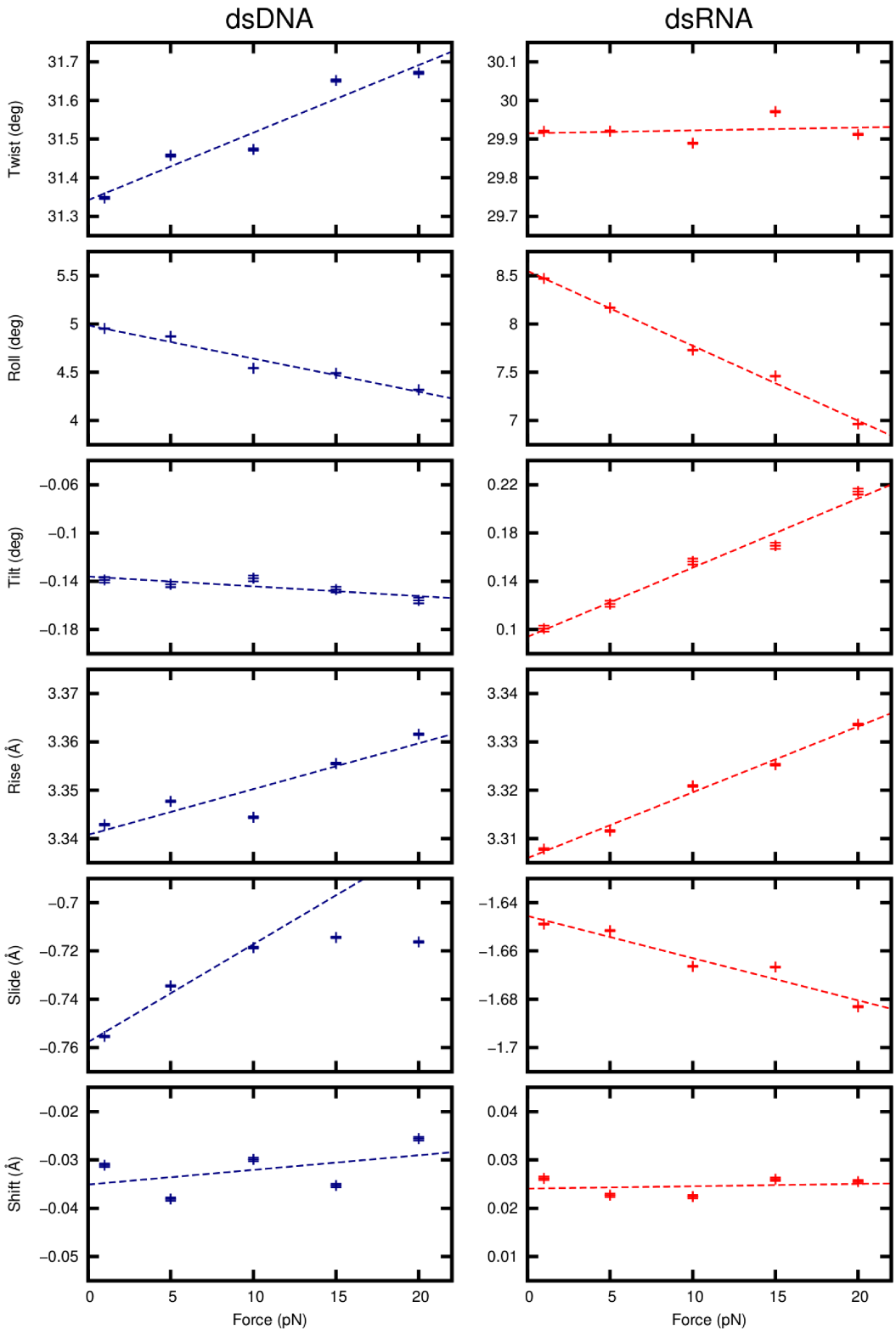

Figure S7: Inter base pair parameters as a function of the force for dsDNA (blue) and dsRNA (red). Error bars are the standard error of the mean. To guide the eye, a linear fit was plotted for all the base pair parameters. Concerning the slide of dsDNA, only the first three points were used in the linear fit.

Figure S8

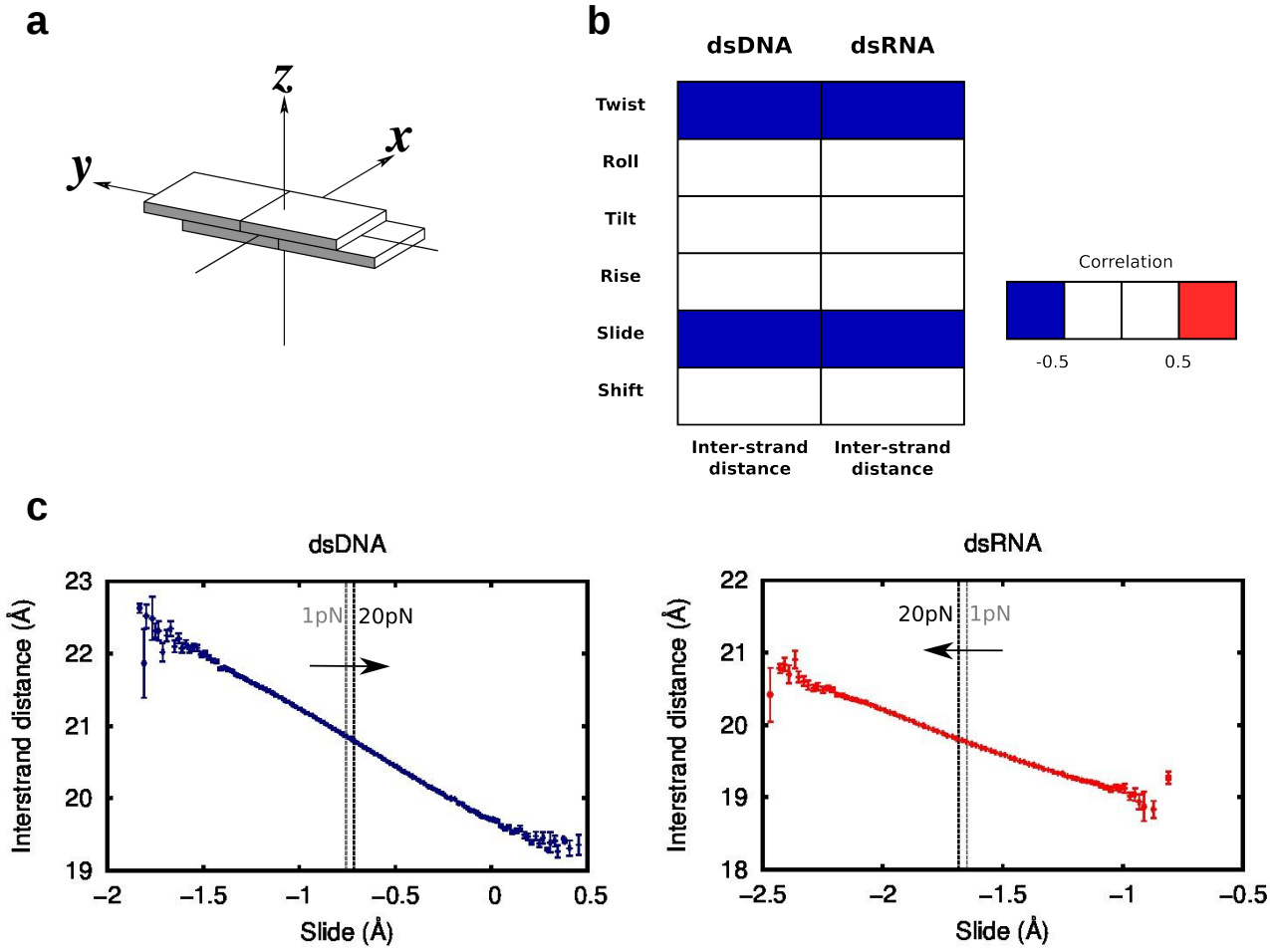

Figure S8: Correlation table and fluctuation of the inter-strand distance with slide. **a**, schematic representation of the slide parameter. **b**, the Pearson correlation factor was computed for the inter-strand distance and each base pair step parameter. The value of the inter-strand distance and base pair step parameter of the ten central base pairs was recorded at every simulation frame at F = 1 pN. Only the twist and the slide parameters showed a correlation higher than 0.5 in absolute value. **b**, fluctuations in the inter-strand distance with the slide at 1 pN force simulation for dsDNA and dsRNA. These two parameters are highly anti-correlated: as the slide approaches zero, the inter-strand distance decreases. Dotted vertical lines represent the mean value of the slide at 1 pN (gray) and at 20 pN (black) force.

Figure S9

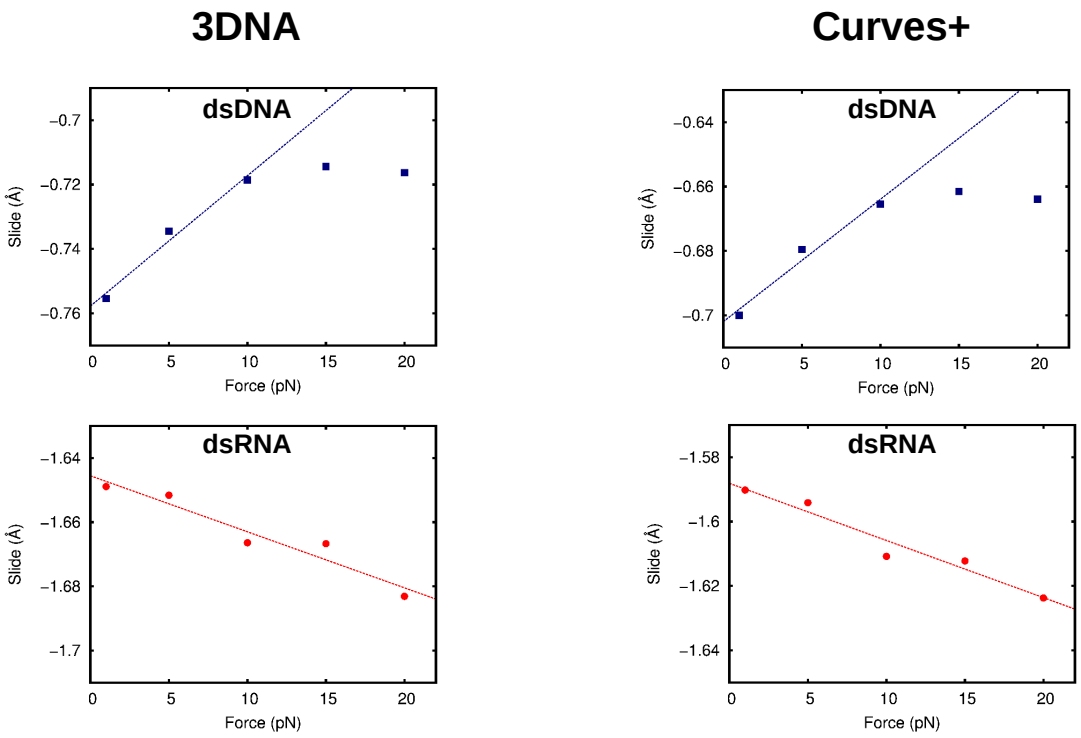

Figure S9: Comparison of the slide base pair step parameter calculated using 3DNA or Curves+ software. The mean slide of the ten central base pairs was computed for each constant force simulation using the 3DNA (left column) and Curves+ (right column) software. A linear fit was performed for the points in the range of 1-10pN in the case of dsDNA and for all the points in the case of dsRNA.

Figure S10

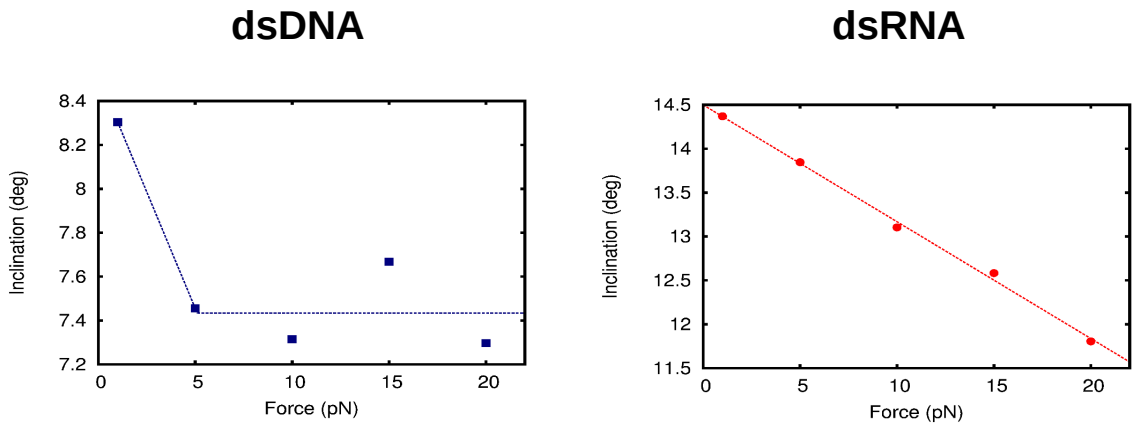

Figure S10: Force-dependence of the inclination parameter measured with Curves+ software. The mean value of the inclination of the ten central base pairs was computed for dsDNA and dsRNA at each constant force simulation. DsDNA points were fitted to a linear function in the 1-5 pN range and to a horizontal line in the 5-20 pN range. DsRNA points were all fitted to a linear function.

Figure S11

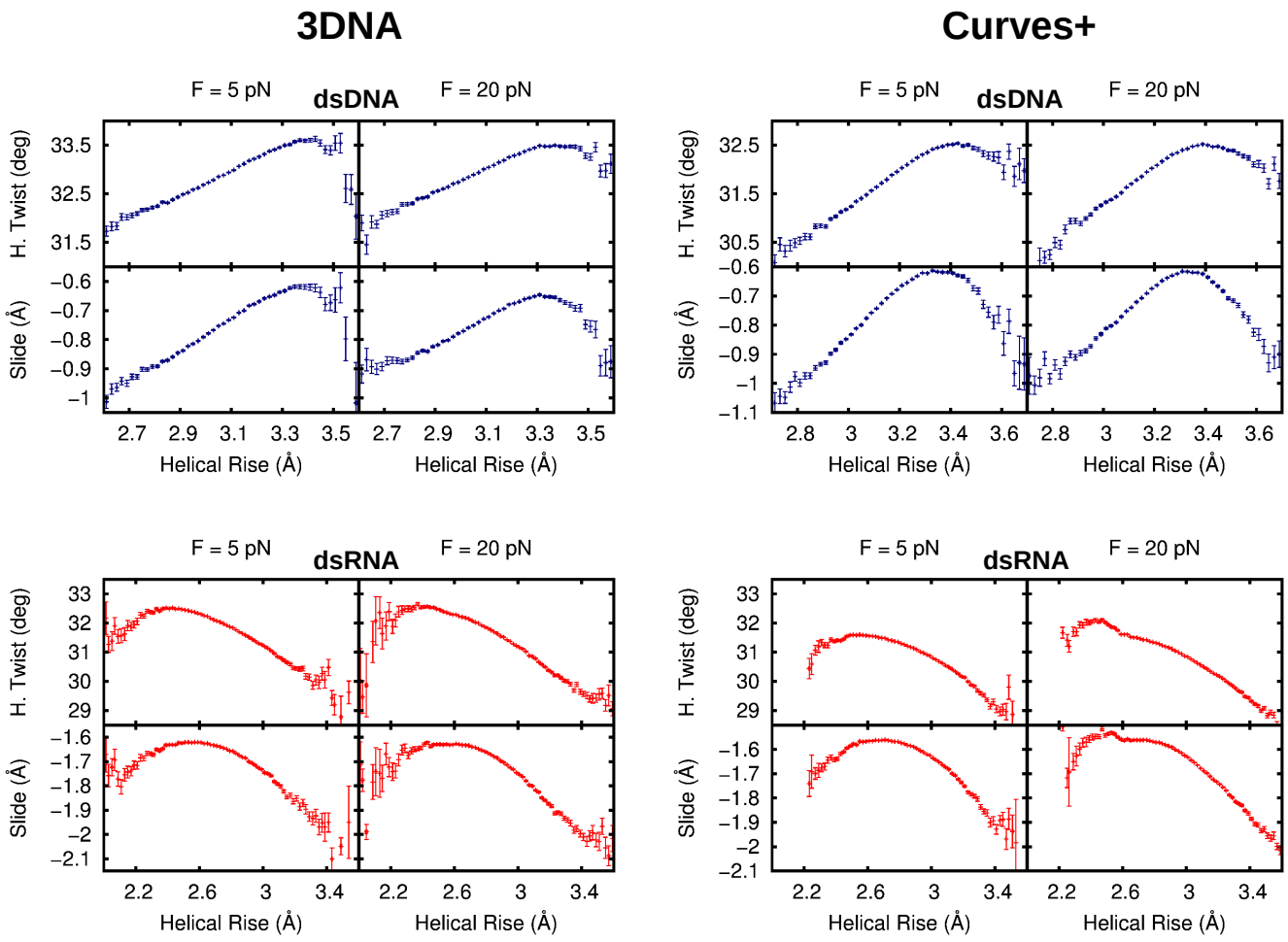

Figure S11: Comparison in the fluctuations in the helical twist and slide with the helical rise at 5 pN and 20 pN simulations for dsDNA and dsRNA calculated using the 3DNA or Curves+ software. The plots in the left column are the same as in **Fig 5a, b** main text. In the right column we represent the same data processed with Curves+.

Figure S12

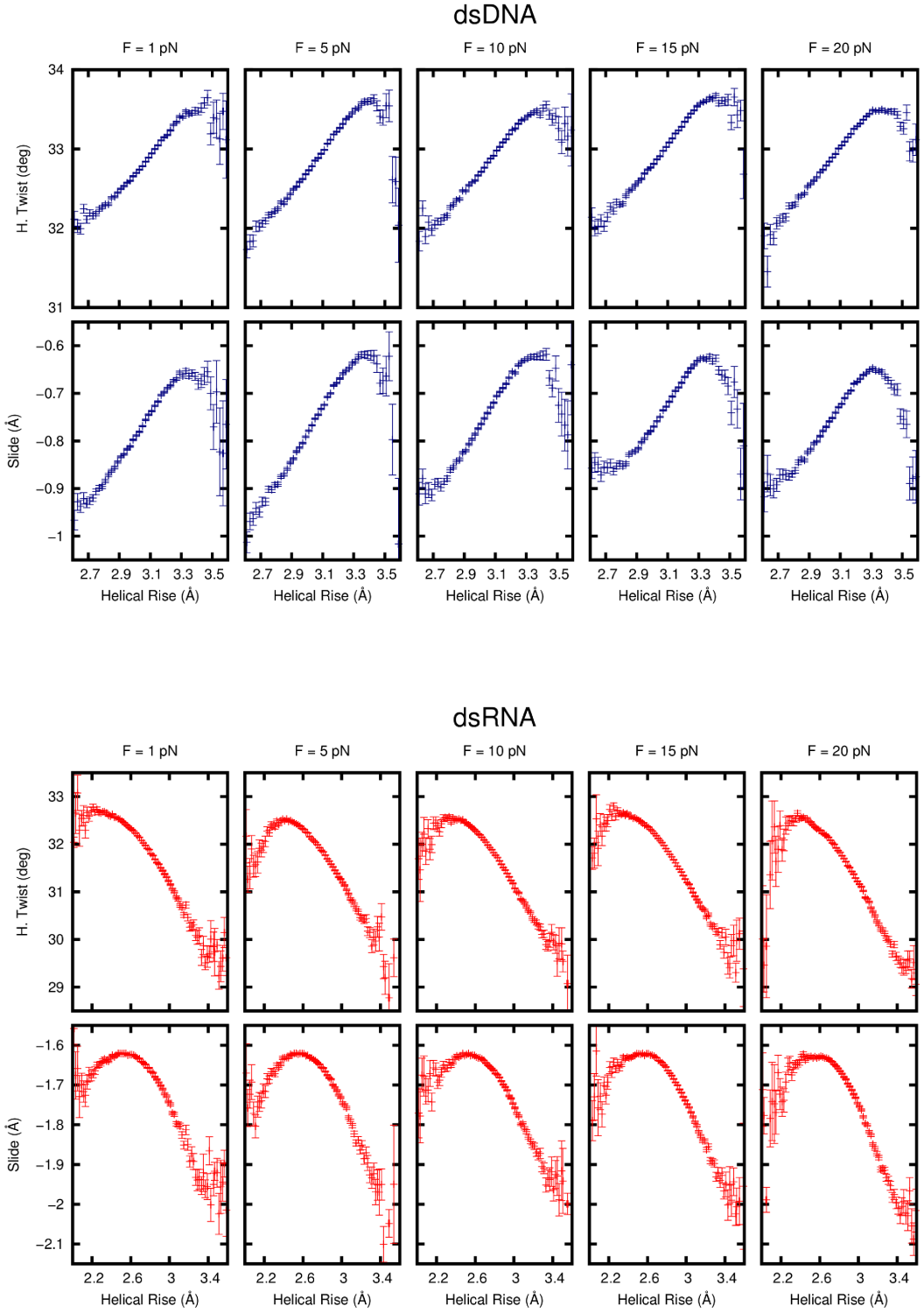

Figure S12: Fluctuations in the helical twist and slide with the helical rise at each constant force simulation for dsDNA (blue) and dsRNA (red). The helical rise was discretized in bins of 0.02 Å and the mean helical rise, helical twist and slide were computed in each bin. Error bars are the standard error of the mean in each bin.

Figure S13

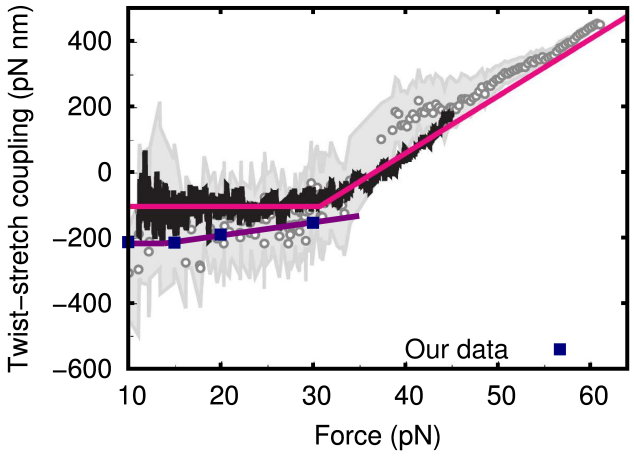

Figure S13: Comparison with experimental results of the force dependence of the twist-stretch coupling. Black line: Twist-stretch coupling obtained in (26) from the measurements performed in (2). Red line: fit of the force-twist curve from (2) using the twistable worm-like chain (tWLC) model proposed in (26). Grey dots: determination of the twist-stretch coupling from force-extension curve using the tWLC model. Blue squares: values of the twist-stretch coupling measured from our simulations. An additional simulation at $F = 30$ pN was performed to confirm the trend of increasing g. Purple line: fit to our data points following the expression for $g(F)$ proposed in (26), i.e., constant g up to a given force, F_c, and linear for forces above F_c. The linear region was extended up to 35pN. Image adapted from (26), with permission from Macmillan Publishers Ltd: Nature Physics, copyright 2011.

Figure S14

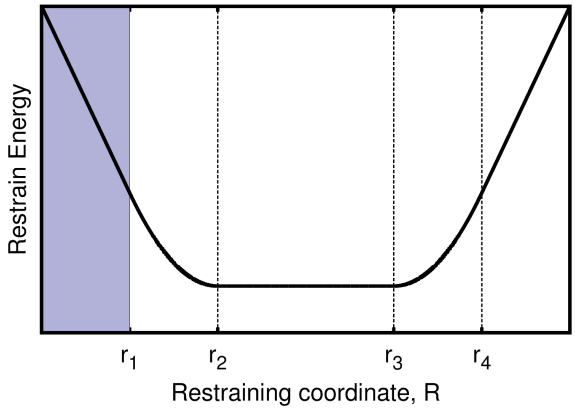

Figure S14: Shape of the restraining potential recently implemented in the *AMBER software package* (7). The parameters r_1, r_2, r_3 and r_4 split the space of the restraining coordinate in five regons. If the restraining coordinate remains in the first region (blue) the potential is linear with negative slope, resulting in a constant stretching force acting on the atoms.